J. Min. Metall. Sect. B-Metall. 59 (2) (2023) 255 - 267

Journal of Mining and Metallurgy, Section B: Metallurgy

EFFECT OF LASER HARDENING ON THE MECHANICAL, TRIBOLOGICAL AND CORROSION PROPERTIES OF LOW ALLOY STEELS

O.A.A. Albahlol [a], H. Cug [a], Y. Akgul [b], A.K. Eticha [a, c], A. Incesu [d,*]

[a] Karabuk University, Mechanical Engineering, Karabuk, Turkey
[b] Karabuk University, Metallurgical and Materials Engineering, Karabuk, Turkey
[c] Addis Ababa Institute of Technology, School of Mechanical and Industrial Engineering, Addis Ababa, Ethiopia
[d] TOBB Tech. Sciences Vocational School, Karabuk University, Karabuk, Turkey

(Received 09 February 2023; Accepted 08 August 2023)

Abstract

This research focuses on studying the mechanical, tribological, and corrosion behaviors of alloy steels: AISI 4340, AISI 5140, and AISI 8620 by laser hardening, respectively. In light of the tests which have been carried out meticulously, it is concluded that the optimum laser hardening parameter for all steel grades is 4 mm/s scanning speed and 1300 °C surface temperature. Micro-structural changes, Vickers hardness as mechanical properties, and tribological properties with reciprocating wear tests were carried out. Furthermore, corrosion tests were conducted. The test results reveal that the maximum hardness is achieved 50-300 µm below the surface for all laser-hardened steels. Additionally, this study demonstrates that the wear resistance of steel is enhanced by the implementation of laser hardening. This study also determines that laser hardening has a positive impact on lifting the corrosion resistance behavior of AISI 4340 steel. In contrast, the corrosion resistance properties of AISI 8620 steel were reduced nearly by 54.17%.

Keywords: *Laser Hardening; Alloy Steels; Mechanical Properties; Wear Resistance; Corrosion*

1. Introduction

Steel, which is a multi-purpose material, is used in construction, aerospace, defense, machinery, automobile, etc. industrial applications [1, 2]. For steel parts, the surface microstructure and composition play a crucial role in determining the surface-dependent engineering properties (corrosion, wear, impact, oxidation resistance, etc.) of the steel in-service conditions. Probably, steel components such as gears, screws, pistons, fasteners, rails, and wheels are subject to wear and surface deformations due to overloading which may cause mechanical losses or corrosion due to aggressive environmental conditions [2]. Therefore, surface modifications due to different applications emerge as a significant research area for steel materials.

Surface treatment techniques such as flame hardening, induction hardening, carburizing, nitriding, carbonitriding, and different hard coating techniques are widely used to improve the wear resistance property of steel materials [3]. These traditional and widely used surface treatment processes have several limitations that include complex heat treatment programs, long time and high energy consumption, no solid solubility limit, larger heat affected zone, slower kinetics, etc. [4].

Laser hardening is the process that will avoid most of the limitations observed in conventional surface treatment used to produce a hard, wear-resistant surface on components by the action of a scanned laser beam for surface hardening of steel with martensitic transformation [5]. When it is compared to traditional hardening operations, laser hardening has such advantages as minimal distortion of parts and no interruption. Moreover, this process is also faster than traditional hardening processes and may be utilized to selectively harden certain areas of components [6]. When laser hardening is compared to traditional hardening techniques such as induction or flame hardening, it is more advantageous in certain aspects. For instance, thanks to laser hardening it is possible to harden the surfaces of complex three-dimensional workpieces and often eliminate the final grinding process due to a minimal heat-affected area [7]. In laser hardening, laser energy of 7-100 Joule/mm^2 is concentrated on the material surface for an interaction time between 0.1 s^{-1} and 10 s^{-1} bringing up the metal

Corresponding author: alperincesu@karabuk.edu.tr

https://doi.org/10.2298/JMMB230209022A

temperature to an austenitizing temperature without making it reach the melting temperature of the steel material [8]. After the laser-material interaction ends, the metal acts as a heat screen to quickly extinguish the heated area [9]. In general, the heating and cooling speed in the laser hardening process is in the range of 10^3–10^4 K/s. Hence, at such fast-cooling speeds, the surface layer is almost completely martensitic. This increases not only the surface wear and corrosion resistance but also the fatigue strength of the workpiece [10].

There are limited studies on the wear, corrosion, and mechanical properties of low and medium-carbon steels that are the most widely used materials in construction and machinery industries by laser hardening. When AISI 4340, AISI 5140, and AISI 8620 are considered, they are the most widely used steel grades in the industry in terms of laser hardening. However, the current studies on them are insufficient. AISI 4340 steel is a medium carbon, low alloy steel known for its toughness and strength in relatively large sections. AISI 8620 steel is a low alloy nickel, chromium, and molybdenum case hardening steel, generally supplied in the rolled condition. AISI 8620 steel offers high external strength and good internal strength, making it highly wear-resistant. 5140 steel plate is widely used in low and moderately-stressed parts for vehicles, engines, and machines where a hard, wear-resisting surface is needed. Fakir et al. analyzed the mechanical behavior of fiber laser heat-treated AISI 4340 steels. The mechanical behavior of the material was improved with the hardening process of a cylindrical workpiece which was made up of 4340 steels with a 3kW fiber laser welding. Thus, the test resulted in more than a 40% increment in fatigue resistance with an average stress interval of less than 0.30% depending on laser hardening [8]. In another study, the effect of laser treatment parameters on surface modification and tribological behavior of AISI 8620 steels was examined by Sougata Roy et al. The effect of different protective gas and laser scanning rates on retained austenite content and tribomechanical properties of AISI 8620 steels were investigated. Based on the results, it was reported that controlling the retained austenite below 10% with an appropriate selection of power density and scanning velocity levels was possible. The oxygen content in the air indicated higher friction levels due to the shearing of oxide layers in the air-protected samples and hence, results in a higher surface roughness [11].

In this study, the mechanical, tribological, and corrosion properties of three different laser-hardened alloy steels (AISI 4340, AISI 5140, and AISI 8620) were investigated. The wear resistance characteristics of both base forms and their laser-hardened forms were studied by applying image processing techniques using MATLAB which has never been applied before for worn surfaces.

2. Experimental

2.1. Laser Hardening Process

The thermal treatments for surface hardening were performed using a 1.2 kW high-power diode laser (Laserline, model LDF-3000-100, Germany), with a wavelength range of 900 nm to 1,080 nm LLK-D/Auto type laser fiber and an elliptical spot of 0.6 and 1.9 mm along the minor and major axes, respectively. The focal distance of the laser to the sample surfaces was 195 mm. The chemical compositions of commercial low alloy steels that were treated with laser surface hardening are given in Table 1. However, instead of all elemental contents, only some elements are included in the table to show the elemental differences between steel grades.

The laser hardening process was applied at 1200, 1250, and 1300 °C surface temperatures at 4 mm/s and 6 mm/s scanning speeds. Parameters were encoded from numbers 1 to 6. Table 2 indicates the laser hardening process parameters. Round specimens with diameters of 55-80 mm and thicknesses of 7-12 mm were used for laser hardening. All specimens were obtained from hot-drawn round steel bars.

Table 2. *Laser hardening process parameters*

Parameter No	Laser Scanning Speed (mm/s)	Surface Temperature (°C)
1	6	1300
2	6	1250
3	6	1200
4	4	1300
5	4	1250
6	4	1200

Table 1. *Nominal and actual chemical composition of steels (wt.%)*

Steel Grade Designation	C	Mn	Ni	Cr	Mo
AISI 4340 (nominal) [12]	0.38-0.43	0.60-0.80	1.65-2.00	0.70-0.90	0.20-0.30
AISI 4340 (actual)	0,42	0.76	1.75	0.83	0.26
AISI 5140 (nominal) [12]	0.38-0.43	0.70-0.90	-	0.70-0.90	-
AISI 5140 (actual)	0,40	0.89	0.02	0.84	0.02
AISI 8620 (nominal) [12]	0.18-0.23	0.70-0.90	0.40-0.70	0.40-0.60	0.15-0.25
AISI 8620 (actual)	0.19	0.73	0.65	0.48	0.16

Laser hardening heat treatment was carried out on the steel samples as per the values of process parameters expressed in Table 2. Subsequently, hardened steel samples were examined using a Nikon Shuttle Pix P-400R model stereo microscope.

2.2. Characterization

Metallography techniques were applied to samples for visual analyses such as the stereo microscope, optical light microscope, and scanning electron microscope for micro-structural characterization. Steel samples were ground with 200 to 2500 mesh abrasive SiC papers and then polished with 3µm and 1µm diamond pastes. Then, they were etched with 5 vol.% Nital solutions. Following metallographic steps, the Nikon Shuttle Pix P-400R model stereomicroscope was utilized to detect the laser-hardened areas. The microstructures of samples were examined by Nikon MA 200 optical light microscope and Carl Zeiss Ultra Pus scanning electron microscope. The OES spectra were collected by an optical emission spectrometer (GNR Atlantis) with the spectral region of 120–800 nm for actual chemical composition analysis of the steels (given in Table 1).

2.3. Mechanical and Chemical Performance Analysis of Laser-Hardened Steels

Vickers hardness tests were performed at a certain depth from the surface under a load of 9.81N using Shimadzu micro-hardness measuring devices. For tribological studies, wear tests were carried out in the UTS Tribometer T10/20 brand reciprocating wear tester machine. This machine works in a linear back-and-forth motion type under loads of 30 N and 60 N for a total of 50 m. The cross-sectional front view micrographs of worn surface areas were measured according to ISO 4287-1997 standard with Mitutoyo SJ-410 surface roughness device [13]. Then, the top view micrographs of the worn surface areas were taken by a Nikon Shuttle Pix P-400R model stereo microscope. Thereafter, the stroke length of the worn surface was determined numerically by using the worn surface area micrographs obtained from stereo microscope devices through image processing techniques using MATLAB. In addition, the following laser hardening process materials were tested for potentiostat-dynamic corrosion using Parstat 4000 Potentiostat Galvanostat with a reference electrode Ag/AgCl in a 3.5% NaCl solution.

3. Results and discussions

3.1. Laser Hardening Optimization

These cross-sectional stereo micrographs of laser-hardened AISI 4340, AISI 5140, and AISI 8620 steel samples are depicted below in Fig. 1-3. Additionally, these figures show the width and depth of the laser-hardened areas.

Fig. 1, Fig. 2, and Fig. 3 show laser-hardened AISI 4340, 5140, and 8620 plates of steel produced according to a) Parameter 1, b) Parameter 2, c) Parameter 3, d) Parameter 4, e) Parameter 5, and f) Parameter 6, respectively. Studies showed that the increase in surface temperature and decrease in

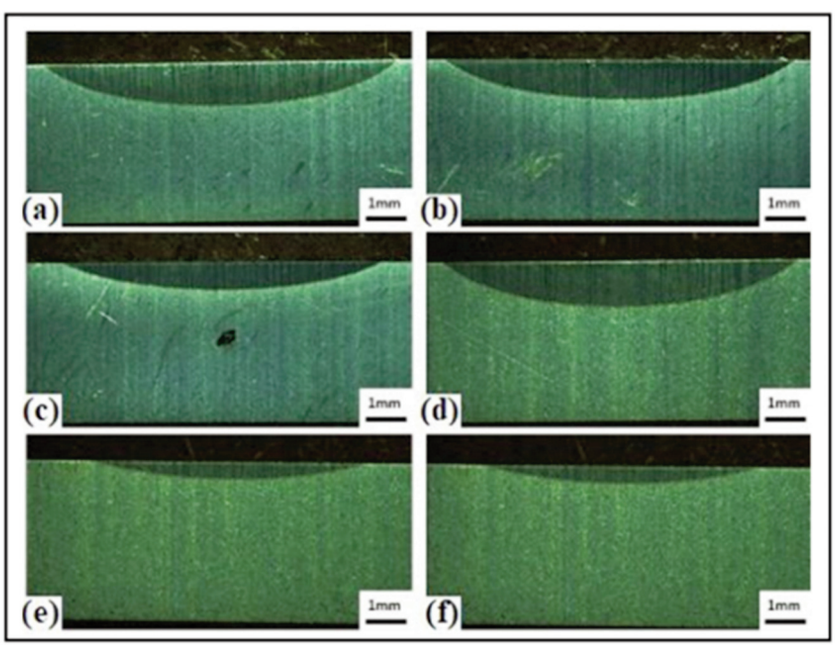

Figure 1. *Laser hardened AISI 4340; laser hardened plates of steel produced according to a) Parameter 1, b) Parameter 2, c) Parameter 3, d) Parameter 4, e) Parameter 5, and f) Parameter 6, respectively*

scanning speed results in the depth of the hardened area that increases more than its width, which leads to an increase in the heat-treated area [11, 14]. As shown in Fig. 1d, Fig. 2d, and Fig. 3d, the largest laser-hardened area formation was observed at the surface temperature and with a lower scanning speed. According to these results, it was concluded that samples produced with parameter 4 (4 mm/s and 1300 °C) showed optimum properties in the processes. Hence, characterization and further studies were applied on steels that laser hardened by this optimized parameter of 4 mm/s scanning speed and 1300 °C surface temperature.

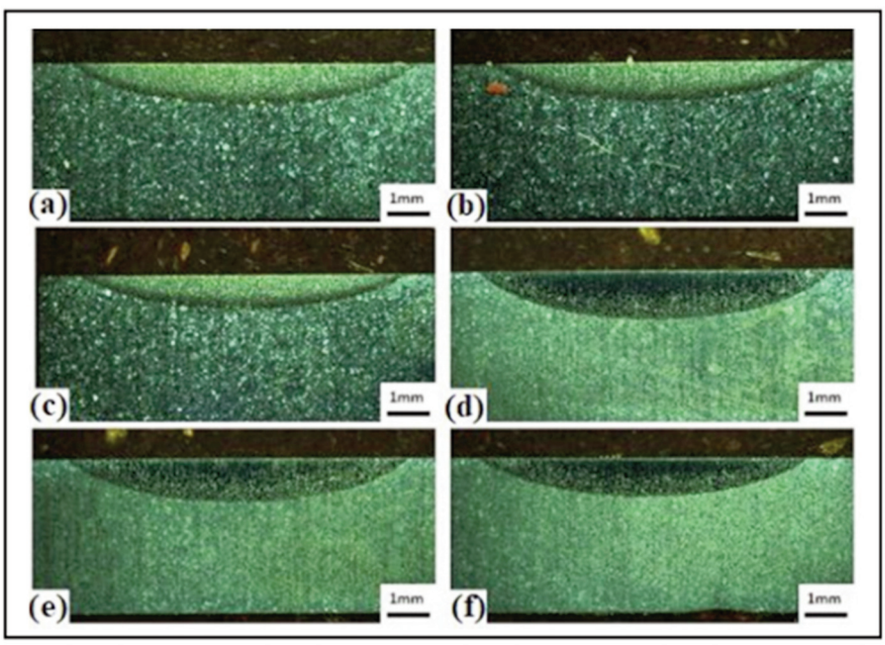

Figure 2. *Laser hardened AISI 5140; laser hardened plates of steel produced according to a) Parameter 1, b) Parameter 2, c) Parameter 3, d) Parameter 4, e) Parameter 5, and f) Parameter 6, respectively*

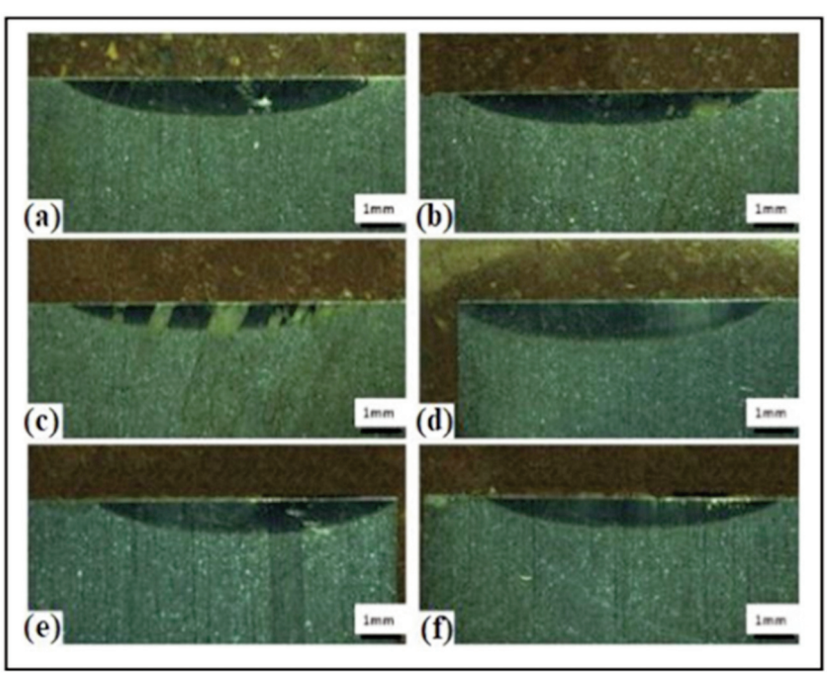

Figure 3. *Laser hardened AISI 8620 steel; laser hardened plates of steel produced according to a) Parameter 1, b) Parameter 2, c) Parameter 3, d) Parameter 4, e) Parameter 5, and f) Parameter 6, respectively*

3.2. Microstructures of Laser-Hardened Steels

Microstructural studies were carried out after laser surface hardening heat treatment using optimum parameters of the laser scanning speed of 4 mm/s and surface temperature 1300 °C. Thus, the surface temperature and carbon content affected the type of microstructure produced within a material [15]. Figs. 4(a) and 4(b) show the stereo cross-sectional micrograph and microstructure of the laser-hardened area of AISI 4340, respectively. In the laser hardening process, decarburization was discovered on the surface of the hardened area as indicated in Fig. 4(c). As a result, hard cementite carbide particles were formed below the surface of the hardened area and carbon content was reduced on the surface. Martensitic (top) and a combination of ferritic and pearlitic (bottom) microstructures were observed at the transition area shown in Fig. 4(d). After the laser hardening process, high cooling rates resulted in martensitic microstructures. This is shown in Fig. 4(e) where martensitic microstructures were revealed in the middle-hardened area. Moreover, ferritic and pearlitic microstructures were seen on the base AISI 4340 steel as seen in Fig. 4(f). These microstructural results are coherent with previous studies [16].

Fig. 5(a) represents the cross-section micrograph of the laser-hardened area of AISI 5140 steel. Here, cementite carbides (dark dots), retained austenite, and martensitic microstructures in the hardened area are observed in Fig. 5(b). Fig. 5(c) depicted below indicates the middle part of the laser-hardened area. Fine grains of bainite and austenitic microstructures were represented in Fig. 5(d). Here in Fig. 5(d), the bainite microstructure was identified by dark features which were formed from austenite under non-equilibrium conditions at temperatures between 250-550 °C. Furthermore, bainite and ferrite microstructures also appear in Fig. 5(e). The bainite is a very fine aggregate of α-phase and Fe_3C (cementite) phases.

Fig. 6(a) indicates the cross-sectional microstructure of the laser-hardened area of AISI 8620 steel. Due to the effect of decarburization, the cementite carbides were formed again on the surface of the hardened area of AISI 8620 as shown in Fig. 6(b). Martensitic and retained austenite microstructures are seen in Fig. 6(c) as well. The red arrow shows the retained austenitic microstructure in Fig. 6(c). Dark gray with irregular shape grains are observed in Figs. 6(d) and 6(e) are pearlitic microstructures.

When the laser scanning speed decreases, the heat input increases to a higher surface temperature. A rapid cooling characteristic following heating transforms the surface layer into a martensite structure almost completely [10]. Therefore, Fig. 6 shows martensitic and retained austenite microstructures on the hardened surface of AISI 8620 steel. The microstructure results demonstrated in Fig. 6 align with previous studies [11, 17]. When the laser heat treatment ends carbon diffusion is limited during decarburization due to the effect of a high cooling rate and lower temperature. Consequently, austenite microstructures remain (retained austenite) without transforming to martensite [17]. Relatively higher temperatures occurred at the surface which enhances the diffusion of carbon atoms.

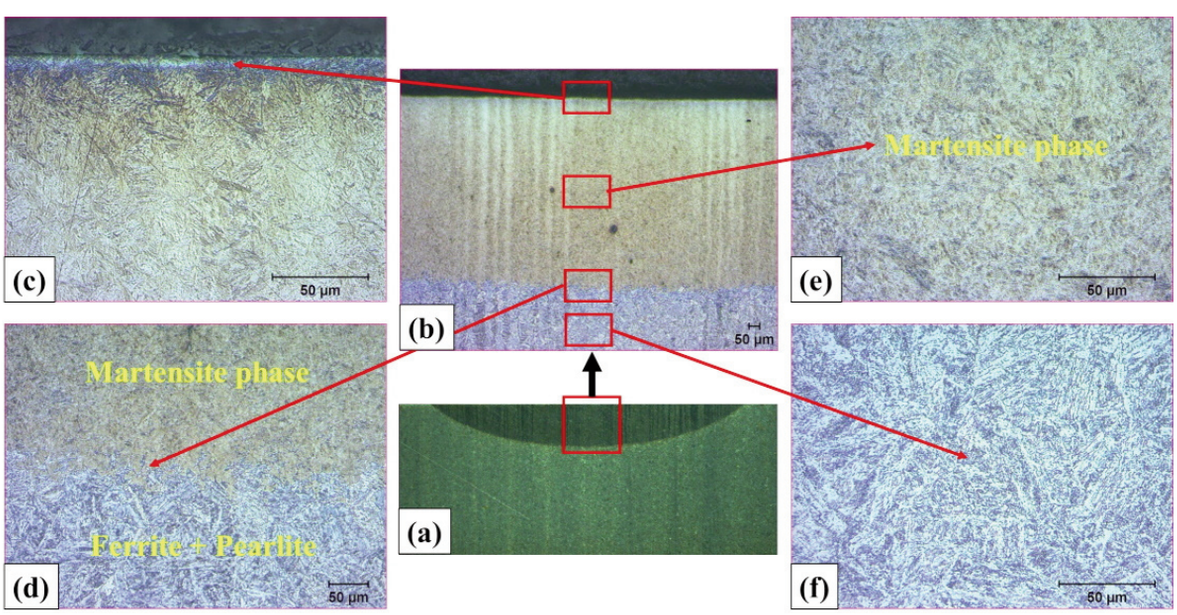

Figure 4. *AISI 4340-Laser Hardened Steel micrographs: a) stereo micrographs of laser hardened AISI 4340, b) general representation of the microstructure of laser hardened AISI 4340, c-f) detailed representation of the microstructure of laser hardened AISI 4340*

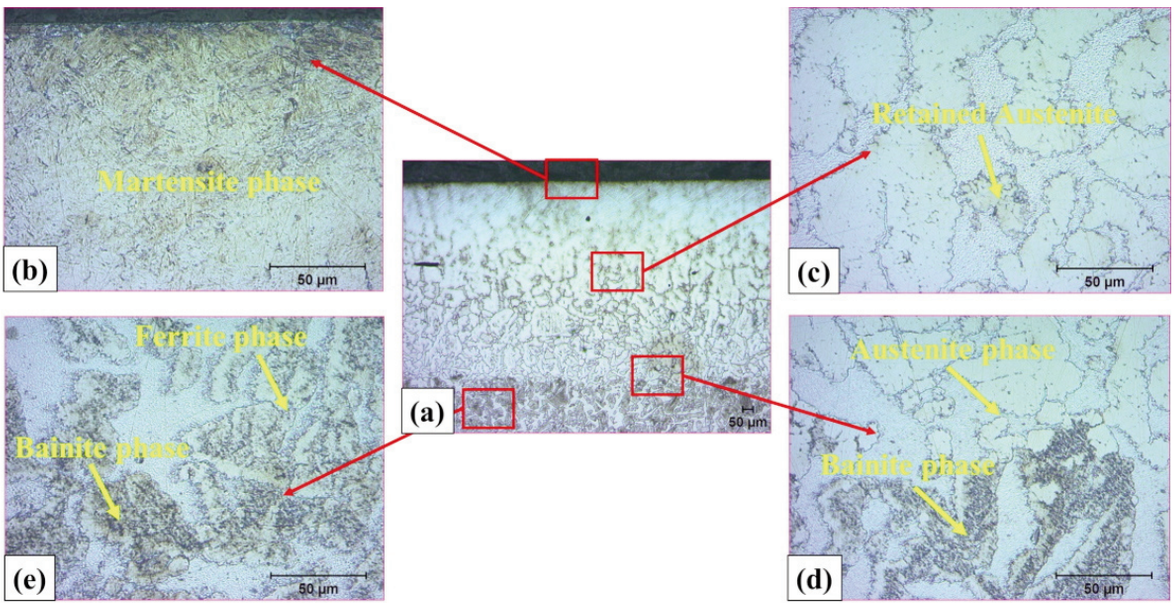

Figure 5. *AISI 5140-Laser Hardened Steel micrographs: a) general representation of the microstructure of laser hardened AISI 5140, b-d) detailed representation of the microstructure of laser hardened AISI 5140*

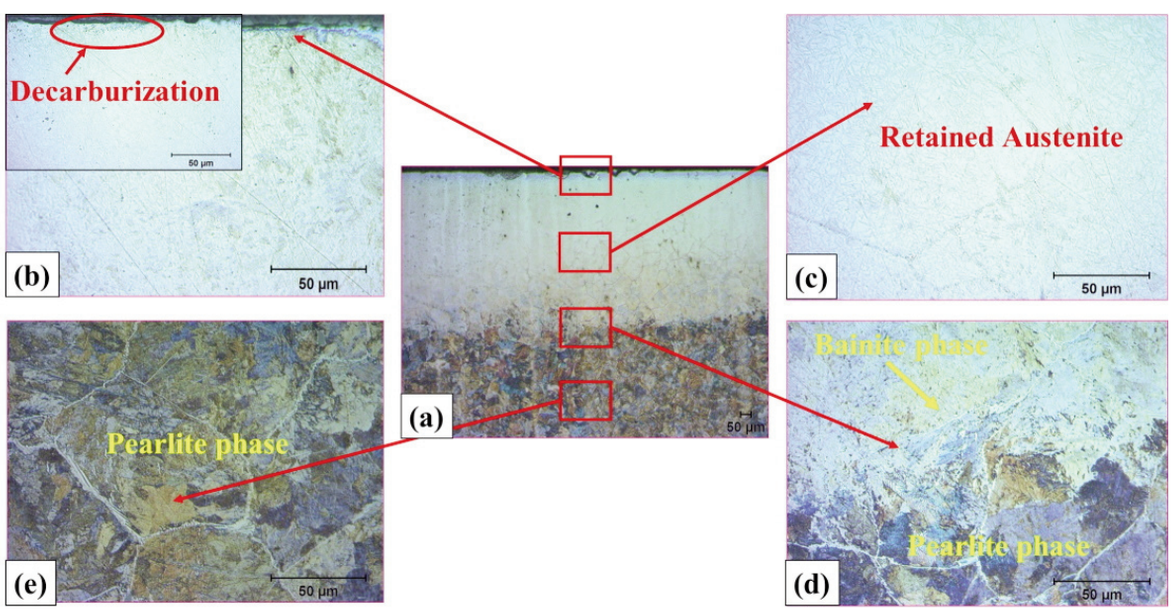

Figure 6. *AISI 8620-Laser Hardened Steel micrographs: a) general representation of the microstructure of laser hardened AISI 8620, b-d) detailed representation of the microstructure of laser hardened AISI 8620*

Thus, these surface temperature assists in microstructure phase transformation. Hence, the retained austenite microstructures are almost completely transformed into martensitic microstructures Fig. 6 (b). This phase transformation occurs within 30-100 µm of the surface in the laser-hardened area as observed in Fig. 6 (c). On the other hand, Fig. 7 shows carbon and iron changes on the surface of the laser-hardened area of AISI 8620 steel. It reveals that there is a carbon difference of 1.84 wt.% between points 1 and 2, confirming the presence of decarburization on the surface of the laser-hardened area. In addition, Figs. 7(b) and 7(c) show changes in the composition of carbon and iron in a 100 µm-hardened area. Likewise, these phenomena are also observed for AISI 4340 and AISI 5140 plates of steel.

3.3. Hardness Test

According to Fig. 8(a), around 30-80 µm below the surface of AISI 4340 and AISI 8620 plates of steel linear increments in their hardness were observed.

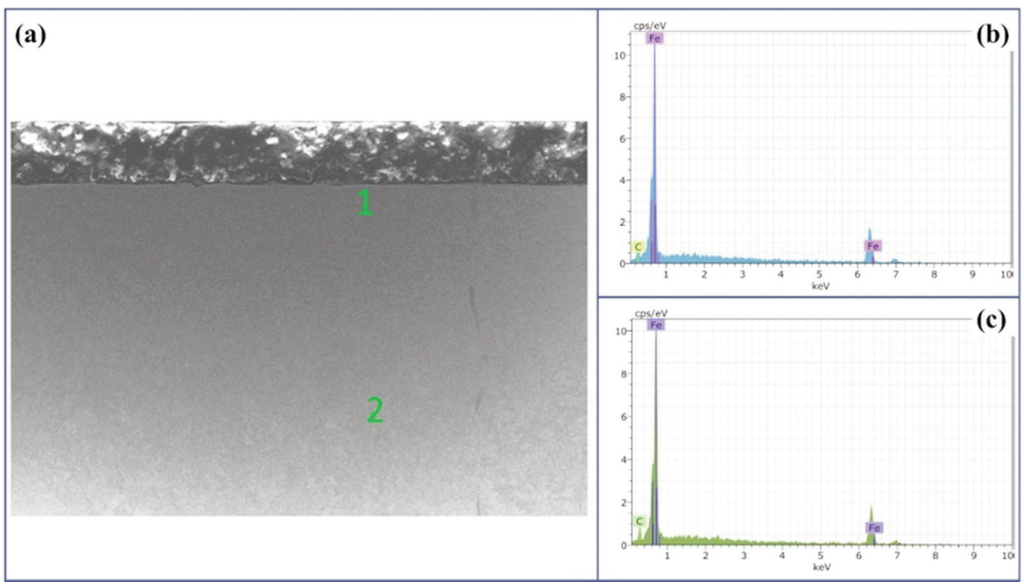

Figure 7. *(a) Point EDX micrograph of laser hardened zone of AISI 8620; (b) carbon and iron ratios of point 1; and (c) carbon and iron ratios of point 2*

Likewise, the maximum hardness for AISI 5140 steel occurred at 300 µm below the surface. Thereafter, the hardness started to decrease as the depth went further away from the surface until it switched from the heat-less zone. Considering Fig. 8(b), when the depth was between 30-80 µm below the surface, the hardness increased from 680-810 HV. Conversely, the hardness linearly decreased to 700 HV as the depth went further to the 450 µm mark. Afterward, it showed a parabolic decrement until it switched to the heat-unaffected area. Decarburization was the main reason for the increment of hardness below the surfaces for all the steels because a decrease in the hardness of steels was expected after decarburization [18]. On the other hand, the main reason for the increase in hardness was the martensitic transformation.

3.4. Wear Test

The worn surface micrographs were captured by a Nikon Shuttle Pix P-400R model stereo microscope. Subsequently, image processing techniques were applied by using MATLAB to determine the stroke length of worn surfaces as displayed in Fig. 9. In the micrograph, the stroke length was measured in terms of 'pixel' scale values.

Figs. 9(a) and 9(b) indicate the stroke length of worn surface AISI 4340-base steel with applied loads of 30N and 60N, respectively. Similarly, the stroke length of the worn surface region for hardened AISI 4340 with 30N and 60N loads are illustrated in Fig. 9(c) and 9(d). The worn stroke length and area of steel were dependent on the applied load and surface hardness.

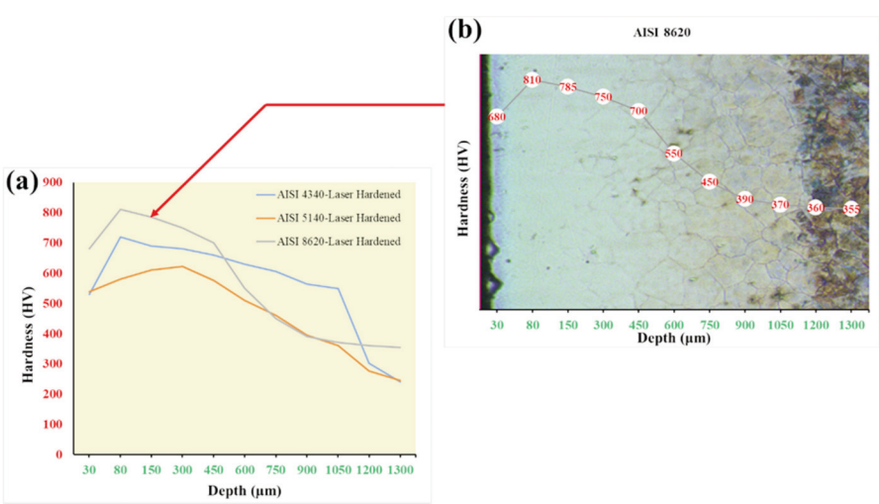

Figure 8. *(a) Hardness versus depth of samples and (b) Hardness versus depth of AISI 8620*

The worn major length and area of AISI 5140-base steel at 30N loads was lower as shown in edge detected Fig. 9(e) than AISI 5140 base at 60N (Fig. 9(f). Fig. 9(g) and 9(h) show worn surface edge detected stroke length of laser-hardened AISI 5140 plates of steel with 30N and 60N loads, respectively. Similarly, Fig. 9(i) and 9(j) show that edge detected worn surface of AISI 8620-base steel, 30N and 60N loads respectively. Moreover, edge detected worn surface area with a determined stroke length of laser-hardened AISI 8620 steels, with applied loads of 30N, and 60N were displayed in Fig. 9(k) and 9(l), respectively.

The cross-sectional micrographs of the worn surface area and depth of steels captured by ISO 4287 standard Mitutoyo SJ-410 device were displayed in Fig. 10. It was found that for the same materials, the base materials have a larger worn surface area than its laser hardened ones. This indicates that surface laser hardening reduced the loss of material from the surface because it is well-known that harder material shows better wear resistance characteristics [19]. Thus, the laser hardening process improved the surface hardness of the steel materials.

As shown in Fig. 11, the wear resistance properties of laser-hardened materials increased for both conditions at 30N and 60N loads for all steels. In addition, a decrease in wear rates was detected. AISI 5140 steel conveyed an increase in the slope of the laser hardening process compared to the base material. However, a decrease in the slope of AISI 8620 steel was discovered in the figure. According to the wear analysis results, the highest wear rate and wear area were observed for AISI 4340 base steel with a 60N applied load of 4.53×10^{-3} mm^3/m and 0.064 mm^2, respectively. Conversely, the lowest wear rate and wear area were recorded for AISI 8620 laser-hardened steel with a 30N applied load of 9.672×10^{-4} mm^3/m and 0.012 mm^2, respectively.

When Fig. 12 is observed, it can be seen that the laser hardening process enhances the wear resistance behavior of AISI 8620 steel in both circumstances i.e., for higher and lower loading conditions compared to other steels. It is because the oxide regions of AISI 8620 are greater than other steels [11], which would reduce the surface roughness created by hard oxide particles (Fig. 12 (f)). Therefore, the small shearing

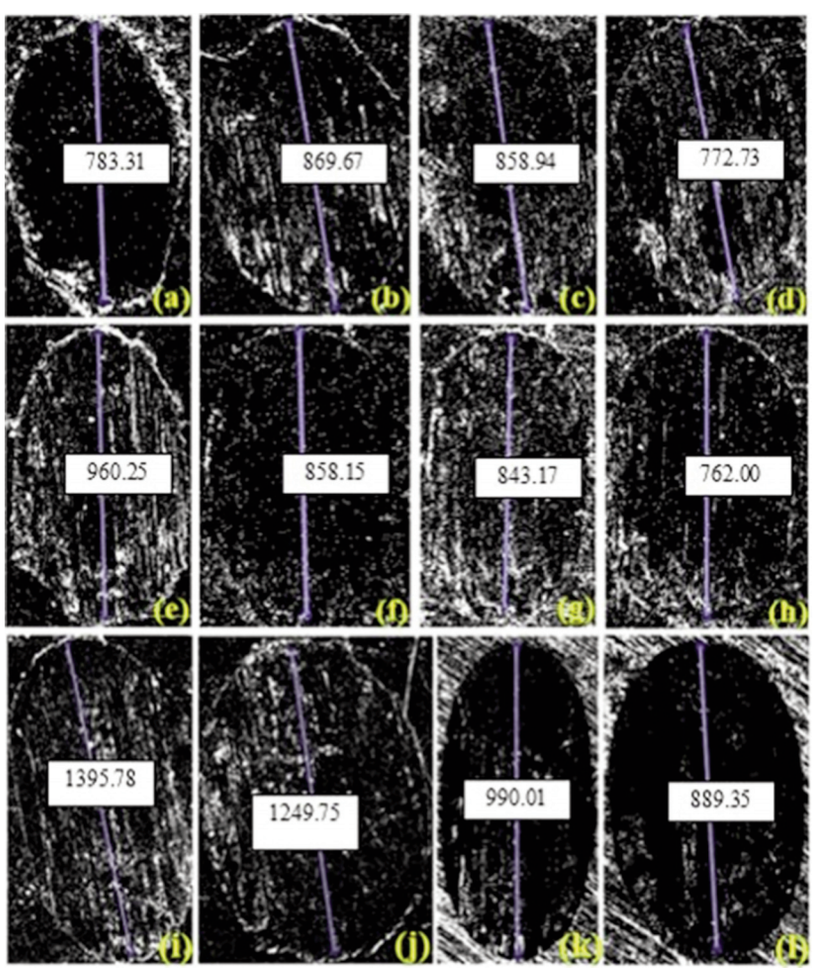

Figure 9. *Stroke length of the worn surface edge detected steels by MATLAB*

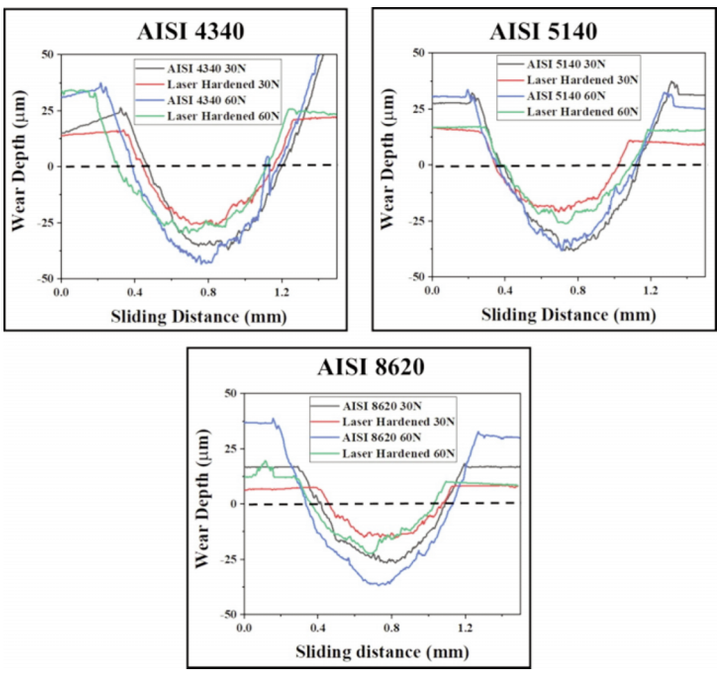

Figure 10. *Wear depth and area of samples*

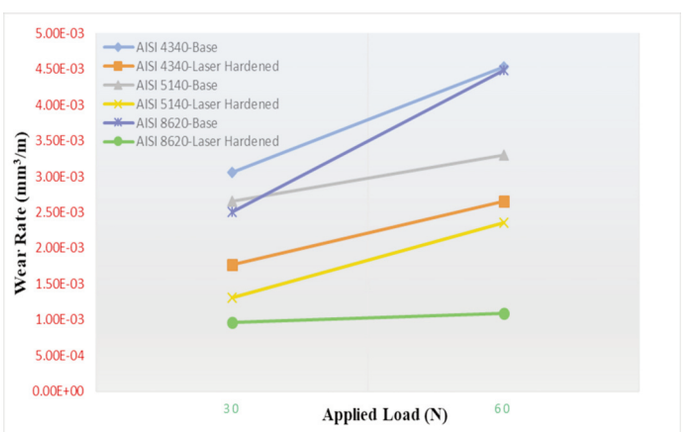

Figure 11. *Wear rate values versus applied loads for the base and laser-hardened samples*

effect among oxide particles results in an improved wear resistance [11] behavior for laser-treated AISI 8620 steel as compared to steels AISI 4340 and AISI 5140. Moreover, the increased temperature of worn surfaces during wear, speed, and amount of reaction with oxygen, and the presence of a certain oxide plate on the material surface can be taken as the reason for the low abrasion wear rate slope of laser treated AISI 8620 steel material. On the other hand, it was observed that the wear rates of samples were increased with increasing applied load. This can be explained by Archard's wear model which presents that wear volume loss is directly proportional to the applied load [20, 21].

Fig. 12, contains worn surface SEM micrographs of base and laser-treated steels of AISI 4340, AISI 5140, and AISI 8620. In general, when comparing AISI 4340 steel and its laser-hardened sample, the result indicates that abrasive wear and oxidative wear are the dominant wear mechanisms as shown in both Fig. 12(a) and 12(b). This also applies to AISI 8620 steel as well. Forming of oxide films can be attributed to occurring of friction heat as a result of reapplied loads [22]. Moreover, the wear mechanism in AISI 5140 steel is observed as both abrasive and adhesive; however, the dominant wear mechanism is adhesive and oxidative wear after laser hardening. In addition, after the laser hardening process, oxide regions in the wear area are visible in the SEM analysis as it appears in Figure 12, and the EDX results of points are

included in Table 3.

Furthermore, considering the worn surface micrographs of laser-hardened samples in Fig. 13 at a 500X magnification, one can deduce that the highest oxide regions appear in AISI 8620 steel, which verifies the lowest wear rate occurred in AISI 8620 steel.

3.5. Corrosion Test

Table 4 shows potentiodynamic corrosion test results. It can be said that the laser hardening process has a positive effect against corrosion by dissolving chromium, nickel, and molybdenum at grain boundaries. Hence, the corrosion resistance characteristics of AISI 4340 steel were improved and doubled. However, it was observed that for AISI 8620 steel corrosion resistance was decreased. It was because cementite carbides in grain and grain boundaries were discontinued after the laser heat treatment. In response to these, the cementite carbide accumulation caused corrosion between grains at the grain boundaries and resulted in a decrease in corrosion resistance [9, 23]. However, there was no significant change in corrosion resistance properties for AISI 5140 steel.

After laser hardening, the corrosion resistance measured value of laser-treated AISI 4340 steel was 0.022 mm/yr., yet it was 0.046 mm/yr. for the base material. It was because the laser hardening process caused the dissolution of corrosion resistance-boosting elements [9, 23]. Conversely, it was seen that

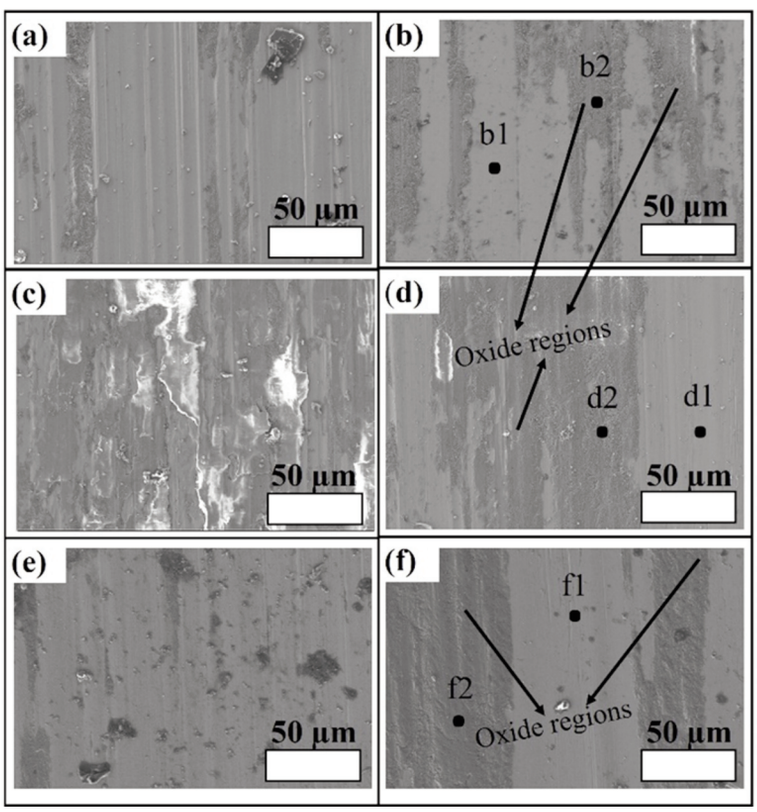

Figure 12. *SEM micrographs of worn surfaces of (a) AISI 4340-Base; (b) AISI 4340-Laser Hardened; (c) AISI 5140-Base; (d) AISI 5140-Laser Hardened; e) AISI 8620-Base; and f) AISI 8620-Laser Hardened*

Table 3. *EDX results after wear test*

	C	O	Si	Cr	Fe	Ni	Mo	Mn
b1	6.12	0.00	0.24	0.63	91.35	1.57	0.10	0.00
b2	11.72	46.48	0.14	0.00	39.76	1.72	0.19	0.00
d1	4.16	0.00	0.74	0.00	93.82	0.00	0.00	1.28
d2	13.70	46.35	0.36	0.28	38.63	0.00	0.00	0.68
f1	5.50	0.00	0.66	2.29	89.20	0.33	0.15	1.88
f2	9.17	45.71	0.11	1.01	42.96	0.28	0.14	0.62

AISI 8620-Laser Hardened steel had reduced corrosion resistance values from 0.022 mm/yr. to 0.048 mm/yr. For this reason, the laser hardening process on AISI 8620 steel had negative effects on its corrosion resistance properties, however, it acted positively on AISI 4340 steel.

Pitting corrosion was observed for both base forms of AISI 4340 and AISI 5140 (Fig.14a and Fig.14b). Pitting occurred at the interface between the primary cementite carbides and the martensitic matrix. It was observed that the pitting corrosion zones decreased after laser hardening application (Fig.14d and Fig.14e). Most of the carbon atoms were used for forming martensite, and the number of cementite carbides in AISI 4340 was lower than that in AISI 5140, which resulted in higher corrosion resistance (Table 4). However, for AISI 8620 pits were scarce and small, and were initiated at the interdendritic boundaries (Fig.14c and Fig.14f), can be understood from the pit morphology, uniform dispersion of fine cementite carbide phases in the matrix, as in both base and laser hardened form of AISI 8620, was a beneficial factor for enhancing the pitting corrosion resistance.

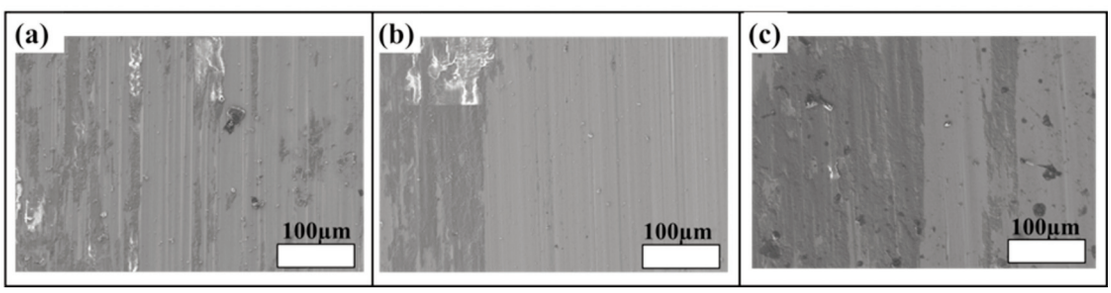

Figure 13. *Wear marks on steels; (a) AISI 4340-Laser Hardened; (b) AISI 5140-Laser Hardened; and (c) AISI 8620-Laser Hardened*

Table 4. *Potentiodynamic corrosion test results*

Specimen	Surface Area (cm^2)	CC (µA)	CCD ($\mu A/cm^2$)	CR (mm/yr.)	Ecorr (V)
AISI 4340-Base	0.126	0.747	5.928	0.046	-0.3729
AISI 4340-Laser Hardened	0.126	0.365	2.896	0.022	-0.3928
AISI 5140-Base	0.126	0.948	7.523	0.058	-0.5277
AISI 5140-Laser Hardened	0.126	0.834	6.619	0.051	-0.4429
AISI 8620-Base	0.126	0.362	2.873	0.022	-0.3751
AISI 8620-Laser Hardened	0.126	0.783	6.210	0.048	-0.3974

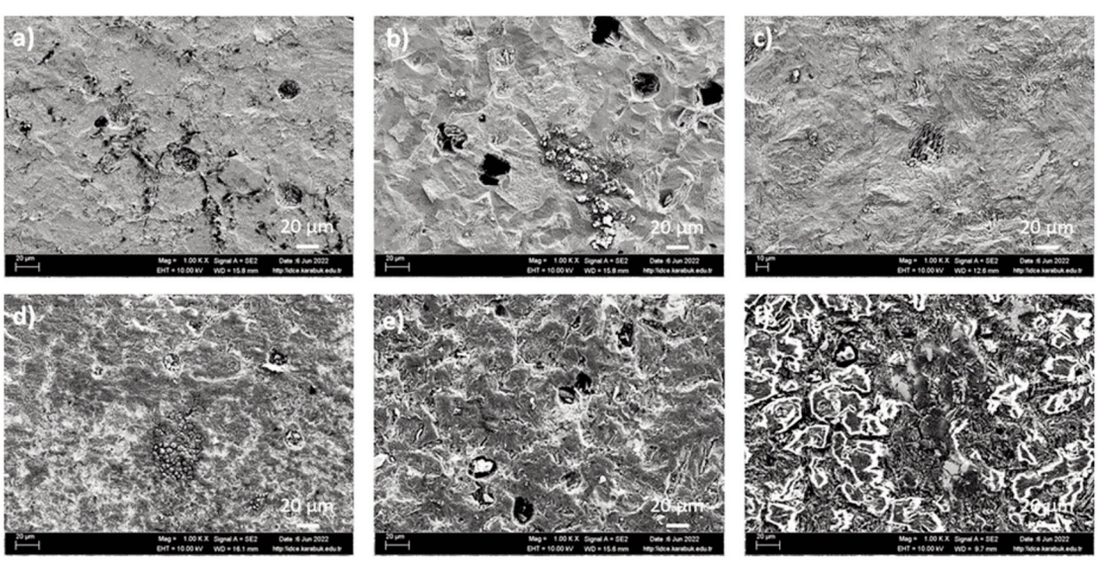

Figure 14. *SEM Micrographs of the alloys after corrosion test; a) AISI 4340-Base, b) AISI 5140-Base, c) AISI 8620-Base, d) AISI 4340-Laser Hardened, e) AISI 5140-Laser Hardened and f) AISI 8620-Laser Hardened*

4. Conclusion

In this study, laser surface hardened AISI 4340, AISI 5140, and AISI 8620 steels were investigated in terms of mechanical, tribological, and corrosion properties, respectively. Following results were obtained:

It was decided that the optimum laser hardening parameter for all steel grades was 4 mm/s scanning speed and 1300 °C surface temperature.

It was determined that retained austenite microstructures had occurred on the steel surfaces due to the fast cooling after the laser hardening process.

The laser hardening process resulted in relatively low surface hardness due to the decarburization phenomenon, and optimum hardness appeared at a depth of 50-300 μm below the surface for all steels.

It was observed that oxide regions on the surface were the decisive factor in wear mechanisms. It was found that the wear rate for all steel-grade steels decreased for all applied loads by laser hardening.

While laser hardening had a reducing effect on the corrosion rate of AISI 4340 and AISI 5140 quality steels, it increased the corrosion rate of AISI 8620 quality steel.

Author's contributions

O.A.A. Albahlol: methodology, writing original draft. H. Cug: conceptualization, writing-review & supervision. Y. Akgul: methodology, writing original draft, investigation. A.K. Eticha: methodology, writing original draft, investigation. A. Incesu: validation, visualization, writing-review & editing.

Data availability

The study did not report any data.

Conflict of Interest

The authors claim that they have no conflicts of interest.

REFERENCES

[1] K. Gao, X. Qin, Z. Wang, S. Zhu, Effect of spot continual induction hardening on the microstructure of steels: Comparison between AISI 1045 and 5140 steels, Materials Science and Engineering: A, 651 (2016) 535–547. https://doi.org/10.1016/j.msea.2015.11.012

[2] G. Muthukumaran, P.D. Babu, Metallurgical characterization of laser hardened, mechanically textured 2.5 Ni-Cr-Mo low alloy steel and optimization using RSM, Optics & Laser Technology, 141 (2021) 107-126. https://doi.org/10.1016/j.optlastec.2021.107126

[3] P.D. Babu, P. Marimuthu, Status of laser transformation hardening of steel and its alloys: a review, Emerging Materials Research, 8(2) (2019), 188–205. https://doi.org/10.1680/jemmr.16.00145

[4] P.D. Babu, G. Buvanashekaran, K.R. Balasubramanian, Experimental studies on the microstructure and hardness of laser transformation hardening of low alloy steel, Transactions of the Canadian Society for Mechanical Engineering, 36(3) (2012), 241–258. https://doi.org/10.1139/tcsme-2012-0018

[5] G. Liu, L. Wang, G. Chen, S. Hua, Parameters optimization of plasma hardening process using genetic algorithm and neural network, Journal of Iron and Steel Research International, 18(12) (2011) 57–64. https://doi.org/10.1016/S1006-706X(12)60010-7

[6] R.S. Lakhkar, Y.C. Shin, M.J.M. Krane, Predictive modeling of multi-track laser hardening of AISI 4140 steel, Materials Science and Engineering: A, 480(1–2) (2008) 209–217. https://doi.org/10.1016/j.msea.2007.07.054

[7] S. Martínez, A. Lamikiz, I. Tabernero, E. Ukar, Laser hardening process with 2D scanning optics, Physics Procedia, 39 (2012) 309–317. https://doi.org/10.1016/j.phpro.2012.10.043

[8] R. Fakir, N. Barka, J. Brousseau, G. Caron-Guillemette, Analysis of the mechanical behavior of AISI 4340 steel cylindrical specimens heat treated with fiber laser, Journal of Manufacturing Processes, 55 (2020) 41–56. https://doi.org/10.1016/j.jmapro.2020.03.039

[9] J. Sundqvist, T. Manninen, H.-P. Heikkinen, S. Anttila, A.F.H. Kaplan, Laser surface hardening of 11% Cr ferritic stainless steel and its sensitisation behaviour, Surface and Coatings Technology, 344 (2018) 673–679. https://doi.org/10.1016/j.surfcoat.2018.04.002

[10] A.K. Nath, A. Gupta, F. Benny, Theoretical and experimental study on laser surface hardening by repetitive laser pulses, Surface and Coatings Technology, 206 (8–9) (2012) 2602–2615. https://doi.org/10.1016/j.surfcoat.2011.11.019

[11] S. Roy, J. Zhao, P. Shrotriya, S. Sundararajan, Effect of laser treatment parameters on surface modification and tribological behavior of AISI 8620 steel, Tribology International, 112 (2017) 94–102. https://doi.org/10.1016/j.triboint.2017.03.036

[12] ASTM A29/A29M; Standard Specifications for General Requirements for Steel Bars, Carbon and Alloy, Hot-Wrought. ASTM International: West Conshohocken, PA, USA, 2013.

[13] Y. Akgul, H. Simsir, Anti-wear behaviour of silver nanoparticles on Al-Si alloy, Surface Topography: Metrology and Properties, 9(2) (2021), 25-31. https://doi.org/10.1088/2051-672X/ac059f

[14] M. Moradi, M. KaramiMoghadam, High power diode laser surface hardening of AISI 4130; statistical modelling and optimization, Optics & Laser Technology, 111 (2019) 554–570. https://doi.org/10.1016/j.optlastec.2018.10.043

[15] B.M. Gurumurthy, S. Sathyashankara, V.S. Ramakrishna, K.U. Achutka, Mechanical characterization and microstructural analysis of AISI 4340 ferrite-martensite dual phase steel, International Journal of Mechanical Engineering and Robotics Research, 8(4) (2019) 553–558. https://doi.org/10.18178/ijmerr.8.4.553-558

[16] G.T.C. Ooi, S. Roy, S. Sundararajan, Investigating the effect of retained austenite and residual stress on

rolling contact fatigue of carburized steel with XFEM and experimental approaches, Materials Science and Engineering: A, 732 (2018) 311–319. https://doi.org/10.1016/j.msea.2018.06.078

[17] T. Mioković, V. Schulze, O. Vöhringer, D. Löhe, Prediction of phase transformations during laser surface hardening of AISI 4140 including the effects of inhomogeneous austenite formation, Materials Science and Engineering: A, 435 (2006) 547–555. https://doi.org/10.1016/j.msea.2006.07.037

[18] C. Zhang, L. Zhou, Y. Liu, Surface decarburization characteristics and relation between decarburized types and heating temperature of spring steel 60Si2MnA, International Journal of Minerals, Metallurgy, and Materials, 20 (2013) 720–724. https://doi.org/10.1007/s12613-013-0789-1

[19] O. Arsun, Y. Akgul, H. Simsir, Investigation of the properties of Al7075-HTC composites produced by powder metallurgy, Journal of Composite Materials, 55(17) (2021), 2339-2348. https://doi.org/10.1177/0021998321990877

[20] M. Raj, K. Manisekar, M. Gupta, Mechanical and wear properties of Mg/Mo nanocomposites, Metallic Materials/Kovové Materiály, 57 (2019) 237–246. https://doi.org/10.4149/km.2019.4.237

[21] M.A. Erden, M.F. Tasliyan, Y. Akgul, Effect of TiC, TiN, and TiCN on microstructural, mechanical and tribological properties of PM steels, Science of Sintering, 53(4) (2021) 497-508. https://doi.org/10.2298/SOS2104497E

[22] Y. Akgul, A. N. Tanrıverdi, M.A. Erden, A novel approach on production of carbon steels using graphene via powder metallurgy, Canadian Metallurgical Quarterly, 61(1) (2022) 85–93. https://doi.org/10.1080/00084433.2021.2023285

[23] A.K. Nath, A. Gupta, F. Benny, Theoretical and experimental study on laser surface hardening by repetitive laser pulses, Surface and Coatings Technology, 206 (8–9) (2012) 2602–2615. https://doi.org/10.1016/j.surfcoat.2011.11.019

UTICAJ LASERSKOG OJAČAVANJA NA MEHANIČKE, TRIBOLOŠKE I KOROZIVNE KARAKTERISTIKE KOD NISKOLEGIRANOG ČELIKA

O.A.A. Albahlol [a], H. Cug [a], Y. Akgul [b], A.K. Eticha [a, c], A. Incesu [d,*]

[a] Univerzitet u Karabuku, Fakultet za mašinsko inženjerstvo, Karabuk, Turska
[b] Univerzitet u Karabuku, Fakultet za metalurgiju, Karabuk, Turska
[c] Institut za tehnologiju u Adis Abebi, Faakultet za mašinsko inženjerstvo i industrijski inženjering, Adis Abeba, Etiopija
[d] TOBB visoka škola za tehničke nauke, Univerzitet u Karabuku, Karabuk, Turska

Apstrakt

Ovo istraživanje se zasniva na proučavanju mehaničkih, triboloških i korozivnih karakteristika niskolegiranih čelika: AISI 4340, AISI 5140 i AISI 8620 prilikom laserskog ojačavanja. Na osnovu pažljivo sprovedenih testova, može se zaključiti da su optimalni parametri za lasersko ojačavanje kod svih vrsta čelika brzina skeniranja od 4 mm/s i temperatura površine od 1300 °C. Izvršene su analize mikrostrukturalnih promena, Vikersove tvrdoće kao mehaničkih karakteristika i triboloških karakteristika koristeći testove recipročnog habanja. Sprovedeni su i testovi za ispitivanje korozivnih karakteristika. Rezultati testova otkrivaju da se maksimalna tvrdoća postiže 50-300 μm ispod površine za sve čelike prilikom laserskog ojačavanja. Osim toga, ovo istraživanje pokazuje da se otpornost na habanje čelika poboljšava primenom laserskog ojačavanja. Takođe se utvrđuje da lasersko ojačavanje pozitivno utiče na povećanje otpornosti na koroziju čelika AISI 4340. Nasuprot tome, svojstvo otpornosti na koroziju čelika AISI 8620 smanjena je za gotovo 54,17%.

Ključne reči: *Lasersko ojačavanje; Legirani čelici; Mehanička svojstva; Otpornost na habanje; Korozija*